Jeong *et al. Applied Biological Chemistry* (2023) 66:82
https://doi.org/10.1186/s13765-023-00840-z

KSABC
The Korean Society for Applied Biological Chemistry

ARTICLE

Open Access

Hypothetical protein CuvA (Rv1422) from *Mycobacterium tuberculosis* H37Rv interacts with uridine diphosphate *N*-acetylglucosamine as a key precursor of cell wall

Yoon Chae Jeong[1], Jihyun Park[1], Yu Jeong Cheon[1] and Ki Seog Lee[1*]

Abstract

Mycobacterium tuberculosis CuvA (Rv1422, MtCuvA) has previously been suggested that it may play a critical role in nutrient utilization and cell wall synthesis required for physiological adaptation in a host cell, but its biochemical details remain unclear. Our previous studies showed that MtCuvA can bind to uridine diphosphate (UDP) sugars as a cell wall precursor component. To verify its functional roles, we report here the biochemical properties of MtCuvA for the binding of UDP-*N*-acetylglucosamine (GlcNAc) using site-directed mutagenesis and docking simulation. The K_D values for UDP-sugars indicate that MtCuvA prefers to bind UDP-GlcNAc as a physiological ligand compared to UDP-glucose. Mutational studies of MtCuvA showed that H12A, T33A, D36A, Q154A, S196, T199A, N226A, and H298A mutants significantly affected the binding to UDP-GlcNAc. We also observed that UDP, but not GlcNAc, could bind to MtCuvA. These results imply that the presence of UDP moiety in the ligand is necessary for interaction with MtCuvA. Moreover, mutational studies of MtCuvA with UDP showed that residues H12, S196, T199, N226, and H298 may be involved in its binding to the UDP moiety, almost consistent with the docking simulation results. Our results provide an insight into the interaction of MtCuvA with UDP-GlcNAc as a key precursor of peptidoglycan.

Keywords *Mycobacterium tuberculosis*, CuvA, Physiological adaptation, Uridine diphosphate *N*-acetylglucosamine, UDP moiety

Introduction

Mycobacterium tuberculosis is the causative agent of tuberculosis (TB), the leading cause of death due to a transmissible disease and drug resistance [1–3]. *M. tuberculosis* possesses a bacterial adaptation ability that can persist for decades despite vigorous host immune responses and environmental changes, thereby adapting its physiological properties to serve interdependent cellular physiological and pathogenic functions [4–7]. Besides, *M. tuberculosis* can utilize a wide range of carbon sources to support its growth in vitro, but in vivo, it resides in intracellular and extracellular niches where nutrient composition and replication are considered to be limited [8, 9]. Nevertheless, to maintain a persistent infection, *M. tuberculosis* must withstand a heterogeneous and continually changing host environment [10]. However, its critical adaptation mechanisms, such as intracellular regulation and reduced bacterial replication to cope with various environmental changes that occur in the host remain unclear. Thus, essential factors involved

*Correspondence:
Ki Seog Lee
kslee@cup.ac.kr
[1] Department of Clinical Laboratory Science, College of Health Sciences, Catholic University of Pusan, Busan 46252, Republic of Korea

in the physiological adaptation that is one of the unique features of *M. tuberculosis* may be an attractive target for discovering new antibiotics against TB.

Mycobacterium tuberculosis CuvA (Rv1422; MtCuvA) is a hypothetical protein predicted to potentially play a critical role in bacterial adaptation [11, 12]. Previous studies have suggested that *M. tuberculosis* Δ*cuvA* mutant may result in defects in cell morphology and sensitivity to cell wall-acting antibiotics, as well as nutrient utilization and establishment of infection in the host cells [11]. Consequently, it has been suggested that MtCuvA may participate in maintaining the structure and/or function of mycobacterial cell wall [11]. Other recent studies showed that *Bacillus subtilis* GlmR (BsGlmR, formerly YvcK), an orthologous protein of MtCuvA, can bind to uridine diphosphate (UDP) sugars, such as UDP-glucose (UDP-Glc) and UDP-*N*-acetylglucosamine (UDP-GlcNAc) [13, 14]. Since UDP-GlcNAc is a precursor for peptidoglycan (PG) synthesis, these results suggested that BsGlmR might be involved in an intermediate step in this process to somehow modulate carbon metabolism or cell envelope homeostasis [13, 15]. Interestingly, MtCuvA has been found in the growing cell pole where new PG biosynthesis occurs in mycobacteria [16], but the roles of MtCuvA in the process of carbon metabolism and cell wall homeostasis are still unclear.

Our previous findings have verified that MtCuvA does not bind NAD(P)$^+$, ADP, or ATP, but can bind to UDP-sugars such as UDP-Glc and UDP-GlcNAc in vitro [12]. Thus, more detailed investigations regarding the interaction of MtCuvA with UDP-sugars are required to improve our understanding of its role in bacterial adaptation including nutrient utilization and cell wall synthesis. In this study, we present the biochemical properties of CuvA (Rv1422) from *M. tuberculosis* H37Rv, which interacts with the UDP-sugars, especially UDP-GlcNAc, as a key precursor for PG synthesis. In addition, we identified key residues involved in the binding of MtCuvA with UDP-GlcNAc and UDP moiety at the putative ligand binding pocket. Our results provide biochemical details regarding interactions of MtCuvA with UDP-GlcNAc as a physiological ligand involved in cell envelope homeostasis.

Materials and methods

Expression and purification of MtCuvA

Wild-type CuvA protein from *M. tuberculosis* (MtCuvA) was overexpressed and purified as described previously [12]. Briefly, the gene encoding CuvA (Rv1422) was amplified by PCR from *M. tuberculosis* H37Rv genomic DNA. The amplified DNA fragment was cloned into the pET-28a vector with a His_6-tag at the *N*-terminus. Recombinant plasmids were transformed into *Escherichia coli* BL21 (DE3), and overexpressed MtCuvA protein was then purified using the Ni^{2+}-chelated HiTrap HP and HiPrep Sephacryl S-200 HR columns (Cytiva). After purification, the soluble fractions containing MtCuvA protein were pooled and concentrated to at least 2.5 mg/ml using an Amicon Ultra-15 centrifugal filter device (Millipore). Protein concentration was estimated using Bradford assay and its purity was confirmed to be > 95% by 15% SDS-PAGE.

Homology modeling and molecular docking simulation of MtCuvA

Analyses of amino acid sequence alignment and secondary structure elements of MtCuvA compared with orthologous proteins, BsGlmR and *Bacillus halodurans* GlmR (BhGlmR) were performed using the *ESPript* 3.0 [17]. Homology modeling of MtCuvA was carried out in the *AlphaFold* 2 [18] and *SWISS-MODEL* workspaces [19] and evaluated based on the QMEAN values compared with the template (PDB entry 2O2Z). For ligands, the 3D structures of UDP and UDP-GlcNAc were applied in docking simulations as the experimental models that might represent the conformation of ligands when bound to the macromolecules. Molecular docking simulations were performed on the *SeamDock* online server [20] using the *Autodock Vina* interface [21], an automated docking tool that predicts how small-size ligands can bind to their binding pocket of proteins. The center of the grid box was set to dimensions of *x*, $z = 0$ Å, and $y = 5$ Å that covered the putative ligand binding pocket. The grid box size was $x = y = z = 20$ Å. The docking simulation was repeated three times with similar parameters to improve the precision of the results. Interactions of protein with ligands were evaluated in terms of minimum binding energy (kcal/mol) for each ligand. Generated results of molecular docking were visualized and depicted using the *PyMol* [22].

Preparation of MtCuvA mutants

Site-directed mutagenesis was performed using the Quickchange mutagenesis method [23], wherein a pair of complementary designed primers (Table 1) were used to amplify the entire plasmid by PCR with a high-fidelity non-strand-displacing *pfu* polymerase. Substitutions for the selected 12 amino acids (H12A, T33A, D36A, R80A, Q154A, S196A, T199A, S200A, N226A, E230A, T295A, and H298A) were introduced into a plasmid DNA encoding wild-type MtCuvA (WT-MtCuvA) that was used as a template for mutagenesis. After digesting the methylated plasmid with *Dpn*I, the mutated plasmid DNA was transformed into competent *E. coli* DH5α cells. All mutants were verified by DNA sequencing. Plasmids containing the desired mutations were transformed into *E. coli* BL21

Table 1 Oligonucleotide primers in forward (F) and reverse (R) directions for site-directed mutagenesis

Primers	Sequences (5′–3′)
H12A-F	CGCGCTGGGCGGCGGAGCCGGCTTCTATGC
H12A-R	CAGCGTCGCATACAAGCCGGCTCCGCCGCC
T33A-F	GTTACCGCCGTGGTGGCGGTCGCCGATGAC
T33A-R	GCCACCGTCATCGGCGTCCGCCACCACGGC
D36A-F	GTGGTGACCGTCGCCGCGGACGGTGGCTCG
D36A-R	GGCCCGACGAGCCACCGTCCGCGGCGACGG
R80A-F	ACTATTCTGCAGCACGCGTTCGGCGGCAGT
R80A-R	ACCACTGCCGCCGAACGCGTGCTGCAGATT
Q154A-F	CGCCTGATCCGTGGCGCGGTGGCGATCGCG
Q154A-R	GTGGTCGCGATCGCCACCGCGCCACGGATC
S196A-F	GTCCTGGGGCCCGGGGCGTGGTTCACCAGC
S196A-R	CACGCTGGTGAACCACGCCCCGGGCCCCAG
T199A-F	CCCGGGTCGTGGTTCGCGAGCGTGATACCC
T199A-R	ATGGGGTATCACGCTCGCGAACCACGACCC
S200A-F	GGTCGTGGTTCACCGCGGTGATACCCCATG
S200A-R	CCAGCACATGGGGTATCACCGCGGTGAACC
N226A-F	CCGCCGTGCCCTGGTGCTCGCCCTGGTGGC
N226A-R	CCCGGTTCAGCCACCAGGGCGAGCACCAGG
E230A-F	GTGCTCAACCTGGTGGCTGCACCGGGAGAG
E230A-R	CCGGCCGTCTCTCCCGGTGCAGCCACCAGG
T295A-F	CGATGTCGCCAGACCTGGTGCACCTTTAC
T295A-R	GCCCGGGTCATGTAAAGGTGCACCAGGTC
H298A-F	CAGACCTGGTACACCTTTAGCTGACCCGGG
H298A-R	CCGCCAGCTTGCCCGGGTCAGCTAAAGGTG

(DE3) strain. MtCuvA mutants were overexpressed and purified using the same protocol as for the wild-type protein. Following purification, purified MtCuvA mutants were concentrated in a buffer containing 50 mM Tris–HCl pH 8.0, 150 mM NaCl, 5 mM β-mercaptoethanol, and 10% glycerol. Protein concentration was estimated using the Bradford assay, and its purity was confirmed to be > 95% by 15% SDS-PAGE.

Thermal shift assay

Thermal shift assay (TSA) was performed using an Applied Biosystems ABI Fast 7500 system. Reaction samples were distributed in 0.1 ml PCR multi-strip (Applied Biosystems, USA) and sealed with cap strips. MtCuvA protein (0.15 mg/ml) was equilibrated with or without each 5 mM of ligand in a reaction mixture (20 µl in each well) containing 5 µl of the Protein Thermal Shift™ buffer (ThermoFisher Scientific, USA) with 2 µl of Protein Thermal Shift™ dye (diluted 10×) (ThermoFisher Scientific, USA). Each melt curve was programmed as follows: 25 °C for 2 min, followed by a 1 °C increase per min from 25 °C to 85 °C, and finally 85 °C for 2 min. Arbitrary fluorescence was plotted as a function of temperature. The melting temperature (T_m) was defined as the temperature with the highest fluorescence, coinciding with the maximum number of dye bindings exposed by thermal denaturation. No significant background fluorescence was observed in the absence of protein. The T_m was analyzed from the melt peak using *Protein Thermal Shift*™ Software v1.4 (Applied Biosystems, USA).

Ligands binding assay of MtCuvA and its mutants

To verify the binding ability of MtCuvA with ligands, thermal shift (ΔT_m) of protein melting temperature induced by the presence of ligands was plotted against the concentration of ligands (0.2–8 mM). The value of ΔT_m was calculated as follows: ΔT_m (℃) = [T_m value of MtCuvA with ligands] – [T_m value of MtCuvA without ligands]. Individual saturation curves were fitted by the following equation $y = \Delta T_m$ max· [L]/(K_D + [L]), where [L] is the concentration of ligand, ΔT_m max is the value when T_m shifted to the maximum. The binding efficiency of ligands was calculated as a ratio of ΔT_m max/K_D. Kinetic parameters were estimated by non-linear square-fit curves for the binding of ligand to MtCuvA using the *SigmaPlot* 10.0 software. All the curves correspond to the average of data from at least four independent experiments and the standard deviations are represented by the error bars.

Results and discussion

UDP-sugars binding to MtCuvA

Our previous studies have verified that MtCuvA can bind to UDP-Glc and UDP-GlcNAc, indicating that its binding to UDP-sugars contributes to their structural stabilization manifested by an increase of T_m on TSA [12]. However, detailed biochemical properties of the interaction between UDP-sugars and MtCuvA remain unknown. To elucidate and quantify these interactions, TSA was performed by monitoring the T_m change (ΔT_m) of MtCuvA in the presence of various concentrations (0.2–8 mM) of UDP-Glc and UDP-GlcNAc. In the effects of UDP-sugars on the T_m of MtCuvA, we found that UDP-Glc and UDP-GlcNAc increased their T_m in a concentration-dependent manner (Fig. 1A and 1B). To evaluate the binding affinity between MtCuvA and UDP-sugars, the K_D value was determined by non-linear least squares-fit curves, representing the ΔT_m of MtCuvA versus the concentration of each ligand (Fig. 1C). The values of K_D for UDP-Glc and UDP-GlcNAc were estimated to be 1.36 ± 0.36 mM and 0.38 ± 0.06 mM, respectively, indicating an approximately 3.6-fold higher affinity for UDP-GlcNAc than for UDP-Glc. In addition, the binding efficiency (ΔT_m max/K_D) of MtCuvA for UDP-GlcNAc was approximately 9.3-fold higher than that for UDP-Glc (Table 2). These results indicate that MtCuvA prefers binding to UDP-GlcNAc

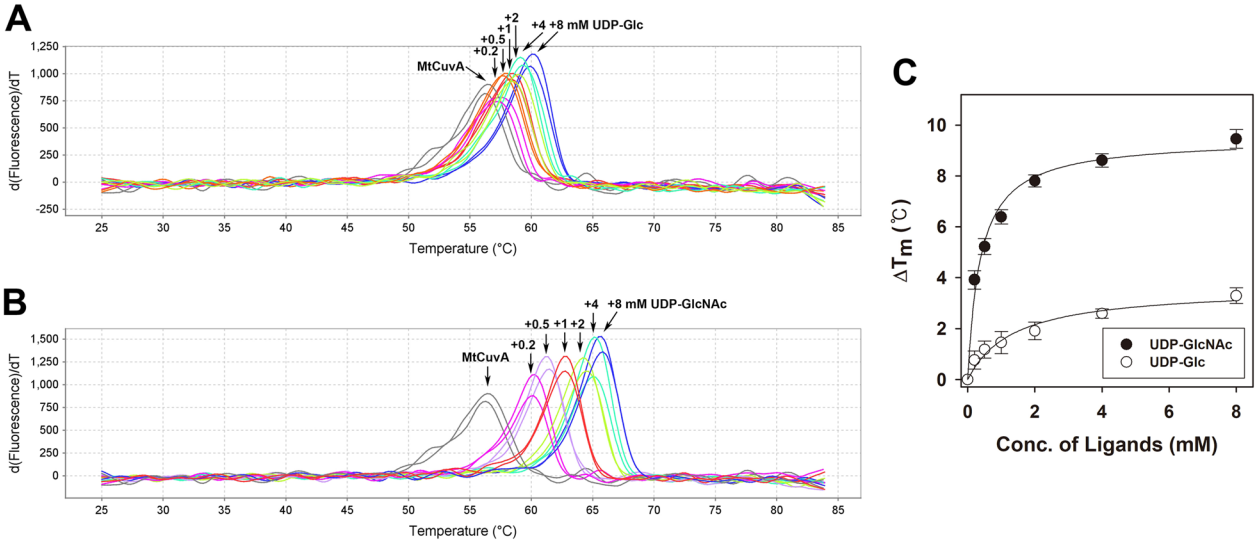

Fig. 1 Analysis of protein thermal shift in the presence of increasing concentrations (0.2–8 mM) of UDP-sugars. MtCuvA melting profiles were monitored in the presence of increasing concentrations of **A** UDP-Glc and **B** UDP-GlcNAc. The melting temperature (T_m) of protein is obtained at the midpoint of each melting curve. **C** Non-linear square-fit curve for the binding of UDP-sugars of MtCuvA. The plots represent the values of ΔT_m for increasing concentrations of UDP-Glc and UDP-GlcNAc, respectively

Table 2 Kinetic parameters for the binding of UDP-sugars to MtCuvA

Variable ligands	K_D (mM)	ΔT_m max	Binding Efficiency (ΔT_m max/K_D)	R^2
UDP-Glc	1.36 ± 0.36	3.64 ± 0.33	2.68 ± 0.75	0.966
UDP-GlcNAc	0.38 ± 0.06	9.47 ± 0.34	24.92 ± 4.04	0.986

R^2 = Coefficient of determination

as a physiological ligand compared to UDP-Glc. Interestingly, recent studies have proposed that BsGlmR, as an orthologue of MtCuvA, might preside over a new mechanism for the regulation of carbon partitioning between central carbon metabolism and PG biosynthesis [24]. Although the detailed mechanisms that may account for the role of MtCuvA in cells remain elusive, these results provide potential evidence that MtCuvA may be involved in a certain process related to PG synthesis to maintain cell wall homeostasis.

Key residues of MtCuvA involved in the binding of UDP-GlcNAc

To compare the ligand binding pocket between MtCuvA and GlmR (YvcK), homology modeling was performed using *AlphaFold* 2 [18] and *SWISS-MODEL* Workspace [19]. The crystal structure of BhGlmR (PDB entry 2O2Z) as an orthologue of MtCuvA was previously determined in complex with NAD^+. However, MtCuvA shares a low sequence identity of approximately 31% with BhGlmR, implying that MtCuvA may have a different conformation in the ligand binding pocket, although it is not yet characterized. The homolog model of MtCuvA obtained from the crystal structure of BhGlmR indicated a high value for the model quality. It was then used to superimpose the MtCuvA model and the BhGlmR structure. Although the overall structure of MtCuvA model was conserved in a similar fold to BhGlmR, the superposition of MtCuvA model with the structure of BhGlmR showed that the conformation of ligand binding pocket differed between BhGlmR and MtCuvA caused by the presence or absence of α-helix (Fig. 2A). To better understand the ligand binding to MtCuvA, molecular docking simulations were performed with UDP-GlcNAc using the *Autodock Vina* interface [21] to predict a putative ligand binding pocket of MtCuvA. Most models of UDP-GlcNAc docked into the MtCuvA model structure appeared at a similar position. The average binding energy of the UDP-GlcNAc model docked to the MtCuvA model structure was estimated to be -8.67 kcal/mol and the best-fit model showed the lowest binding energy of − 8.70 kcal/mol, suggesting that it formed a stable complex (Fig. 2B). Moreover, the best-fit model of UDP-GlcNAc docked into the MtCuvA model suggested that seven residues (H12, D36, D55, S196, T199, S200, and H298) might form hydrogen bonds.

To verify more detailed interaction of MtCuvA with UDP-GlcNAc based on the docking simulation results, we carried out the site-directed mutagenesis of several residues expected to be involved in the binding of UDP-GlcNAc at the putative ligand binding pocket of MtCuvA.

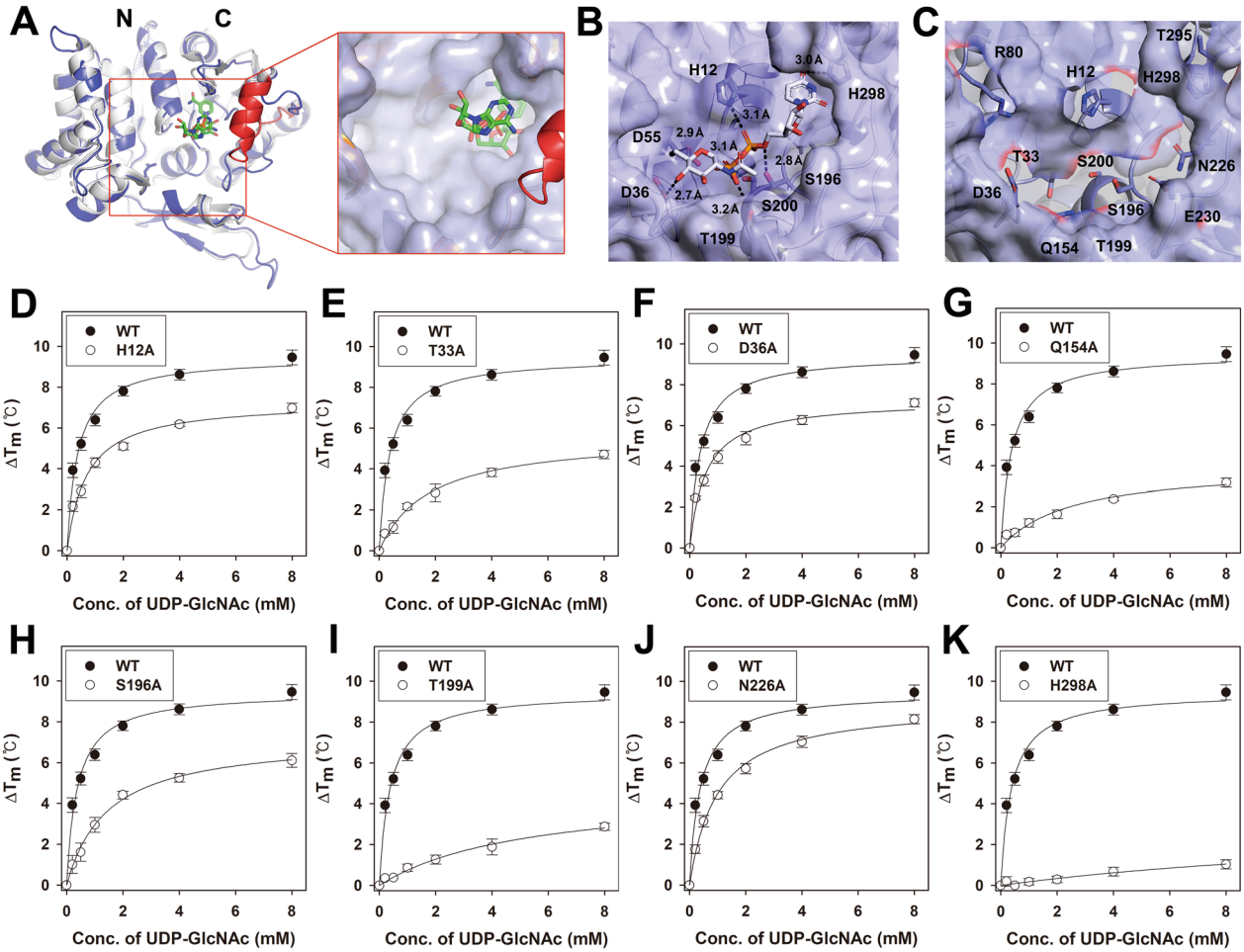

Fig. 2 Identification of key residues of MtCuvA involved in the binding of UDP-GlcNAc. **A** Superimposition of a proposed homology model of MtCuvA with *B. halodurans* GlmR (PDB ID: 2O2Z). Differential conformation is shown in the ribbon shape colored in red. **B** Best-fit model by docking simulation of MtCuvA model with UDP-GlcNAc. Residues suggested to form the hydrogen bonds with the ligand are shown as sticks. The hydrogen bond interactions are indicated by black dotted lines with the distances. **C** Residues were predicted to interact with the ligand in the putative ligand-binding pocket of the MtCuvA model. Residues applied to the site-directed mutagenesis are shown as sticks and colored by element types. **D**–**K** Non-linear square-fit curve for the UDP-GlcNAc binding to MtCuvA mutants. The melting profiles of H12A (**D**), T33A (**E**), D36A (**F**), Q154A (**G**), S196A (**H**), T199A (**I**), N226A (**J**), and H298A (K) were monitored in the presence of increasing concentrations (0.2–8 mM) of UDP-GlcNAc

Previous studies of mutation altering the UDP-sugar binding site in BsGlmR revealed that residues T14, N218, Y265, and R301 (corresponding to the residues that interacted with the NAD^+ in the structure of BhGlmR) may be involved in the binding of UDP-GlcNAc [13]. Despite the low sequence identity, residues in the ligand binding pocket shown in the structure of BhGlmR were conserved at the same positions as MtCuvA except for a few residues. Based on these findings, 10 residues (T33, D36, R80, Q154, S196, T199, S200, E230, T295, and H298) and two residues (H12 and N226 corresponding to T14 and N218 of BsGlmR) were substituted with alanine (Fig. 2C). The K_D value and the binding efficiency (ΔT_m max/K_D) were then estimated using TSA (Table 3). Among these mutants, the K_D values and binding efficiencies for the R80A, S200A, E230A, and T295A mutants were similar to those of WT-MtCuvA, indicating that the mutation of these residues did not affect the binding of UDP-GlcNAc to MtCuvA. On the other hand, H12A, D36A, and N226A mutants slightly affected the binding of UDP-GlcNAc to MtCuvA. The binding efficiencies of these mutants were approximately over twofold lower than that of WT-MtCuvA (Fig. 2D, F and J). In particular, T33A, Q154A, S196A, T199A, and H298A mutants were observed to significantly reduce the binding efficiency for UDP-GlcNAc. The K_D values of T33A, Q154A, and

Table 3 Kinetic parameters for the binding of UDP-GlcNAc to MtCuvA mutants

UDP-GlcNAc	K_D (mM)	ΔT_m max	Binding efficiency (ΔT_m max/K_D)	R^2
Wild type	0.38 ± 0.06	9.47 ± 0.34	24.92 ± 4.04	0.986
H12A	0.69 ± 0.11	7.30 ± 0.32	10.58 ± 1.75	0.986
T33A	1.77 ± 0.24	5.63 ± 0.28	3.18 ± 0.46	0.992
D36A	0.56 ± 0.09	7.24 ± 0.32	12.93 ± 2.15	0.984
R80A	0.50 ± 0.07	9.44 ± 0.31	19.07 ± 2.61	0.990
Q154A	2.48 ± 0.61	4.02 ± 0.41	1.62 ± 0.43	0.976
S196A	1.45 ± 0.14	7.25 ± 0.24	5.01 ± 0.51	0.996
T199A	5.25 ± 1.18	4.66 ± 0.55	0.89 ± 0.23	0.988
S200A	0.20 ± 0.03	10.47 ± 0.30	52.35 ± 7.99	0.988
N226A	0.98 ± 0.09	8.90 ± 0.25	9.08 ± 0.87	0.996
E230A	0.26 ± 0.04	9.38 ± 0.28	36.08 ± 5.65	0.998
T295A	0.37 ± 0.05	9.20 ± 0.29	24.86 ± 3.45	0.990
H298A	ND*	ND	ND	–

R^2 = Coefficient of determination

* ND means "no determined" and indicates that the binding of UDP-GlcNAc to MtCuvA and the Δ T_m values are too weak to calculate the K_D

S196A mutants were approximately 4 to sevenfold higher than that of WT-MtCuvA, and their binding efficiencies were approximately 5 to 15-fold lower than that of WT-MtCuvA (Fig. 2E, G and H). Besides, T199A and H298A mutants strongly affected the binding of UDP-GlcNAc to MtCuvA. The K_D value of T199A mutant was approximately 14-fold higher than that of WT-MtCuvA, and its binding efficiency was approximately 28-fold lower than that of WT-MtCuvA (Fig. 2I). H298A mutant showed too low values of K_D and ΔT_m max to estimate its binding efficiency (Fig. 2K). Taken together, these results indicate that eight key residues (H12, T33, D36, Q154, S196, T199, N226, and H298) may play an important role in the binding of UDP-GlcNAc at the putative ligand binding pocket of MtCuvA.

Identification of the UDP-moiety binding site in MtCuvA

PG, a major component of the cell wall, is continuously reconstructed during growth and cell division and plays a critical role in protecting and shaping most bacteria including mycobacteria. UDP-GlcNAc is one of the key precursors of PG synthesized in the cytoplasm. Previous studies have suggested that BsGlmR may participate in the metabolic regulation regarding the UDP-GlcNAc synthesis [24]. Biochemical properties of BsGlmR regarding its binding to UDP-GlcNAc were reported [13], but detailed information on the interactions with its ligands is still insufficient. Moreover, a structural comparison between the MtCuvA model and the BhGlmR structure showed slight differences in ligand binding pockets. Based on the above results, further investigations are required to verify unique ligand binding properties of MtCuvA to UDP-GlcNAc. UDP-GlcNAc as a physiological ligand of MtCuvA contains two moieties, UDP and GlcNAc (Fig. 3A). To confirm how two moieties of UDP-GlcNAc contributed to structural stabilization of MtCuvA, the binding properties of UDP and GlcNAc were analyzed using TSA. As shown in Fig. 3B, no binding of GlcNAc to MtCuvA was detected, but the binding of UDP increased in the T_m of MtCuvA. The value of K_D for UDP was estimated to be 1.71 ± 0.11 mM, indicating approximately 4.5-fold higher than that of UDP-GlcNAc. The binding efficiency (ΔT_m max/K_D) for UDP was approximately 14-fold lower than that for UDP-GlcNAc (Fig. 3C). Although MtCuvA prefers the binding to UDP-GlcNAc as a physiological ligand compared to UDP, these

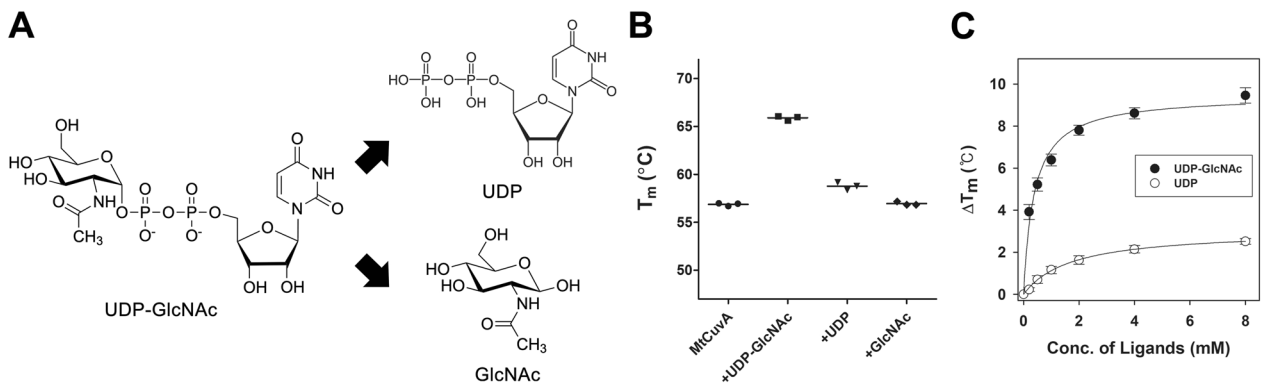

Fig. 3 Binding properties of MtCuvA with two moieties of UDP-GlcNAc. **A** Chemical structures of UDP-GlcNAc and its two moieties (UDP and GlcNAc). **B** The melting temperatures (T_m) of MtCuvA with or without UDP-GlcNAc, UDP, and GlcNAc (each 5 mM). Four replicate reactions were performed on a real-time PCR system using the melt curve by protein thermal shift. **C** Non-linear square-fit curve for the UDP and UDP-GlcNAc binding to MtCuvA using thermal shift assay. The melting profiles were monitored in the presence of increasing concentrations (0.2–8 mM) of ligands

results indicate that the presence of the UDP-moiety in the ligand is essential for its interaction.

To improve our understanding of the binding of UDP to MtCuvA, molecular docking simulations were performed with UDP using the *Autodock Vina* interface [21] in the same manner as UDP-GlcNAc. Models of UDP docked into the MtCuvA model structure appeared in slightly different orientations at the putative ligand binding pocket. Among them, the best-fit model of UDP docked to the MtCuvA model was estimated to be -8.0 kcal/mol, which was found to be located in a similar orientation to that of UDP-GlcNAc, and suggested that seven residues (H12, D55, S196, T199, S200, E230, and H298) might form hydrogen bonds (Fig. 4A). Based on the docking simulation results of the UDP model, the binding properties of UDP to eight mutants (H12A, T33A, D36A, Q154A, S196A, T199A, N226A, and H298A) of MtCuvA that affected its UDP-GlcNAc binding were analyzed for the values of K_D and binding efficiency (ΔT_m max/K_D) using TSA (Table 4). The values of K_D and binding efficiencies for the T33A, D36A, and Q154A mutants were similar to or even better than those of WT-MtCuvA, indicating that these residues may not be involved in the binding

Table 4 Kinetic parameters for the binding of UDP to MtCuvA mutants

UDP	K_D (mM)	ΔT_m max	Binding efficiency (ΔT_m max/K_D)	R^2
Wild type	1.71 ± 0.11	3.06 ± 0.07	1.79 ± 0.12	0.998
H12A	1.85 ± 0.28	2.08 ± 0.12	1.12 ± 0.18	0.991
T33A	1.87 ± 0.13	4.69 ± 0.12	2.51 ± 0.19	0.998
D36A	1.57 ± 0.12	4.88 ± 0.13	3.11 ± 0.25	0.997
Q154A	1.55 ± 0.34	3.21 ± 0.25	2.07 ± 0.48	0.978
S196A	25.20 ± 23.15	6.02 ± 4.43	0.24 ± 0.28	0.974
T199A	5.51 ± 3.28	2.35 ± 0.75	0.43 ± 0.29	0.914
N226A	ND*	ND	ND	–
H298A	ND*	ND	ND	–

R^2 = Coefficient of determination

* ND means "no determined" and indicates that the binding of UDP to MtCuvA and the ΔT_m value are too weak to calculate the K_D

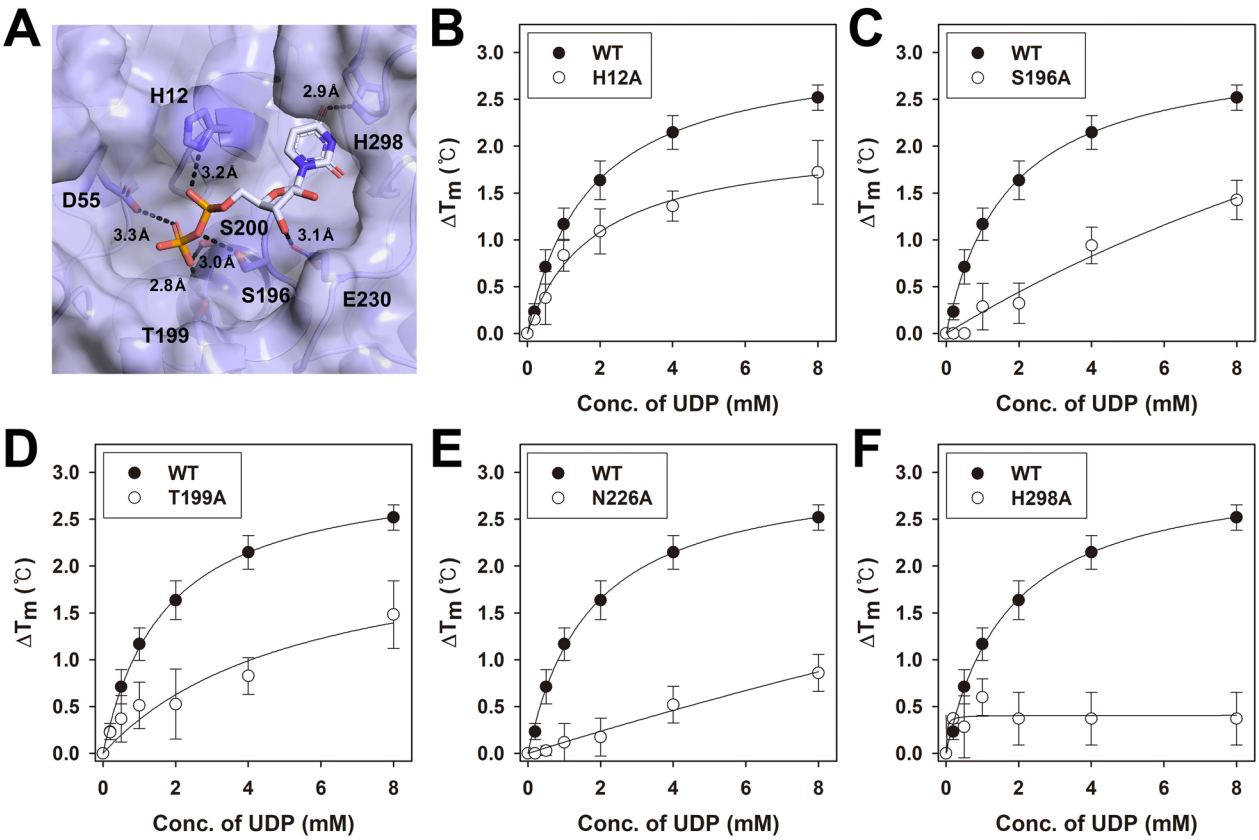

Fig. 4 Binding of UDP moiety to MtCuvA. **A** Best-fit model by docking simulation of MtCuvA with UDP-moiety. Residues suggested to form the hydrogen bonds with the ligand are shown as sticks. The hydrogen bond interactions are indicated by black dotted lines with the distances. **B**–**F** Non-linear square-fit curve for the UDP binding to MtCuvA mutants. The melting profiles of H12A (**B**), S196A (**C**), T199A (**D**), N226A (**E**), and H298A (**F**) were monitored in the presence of increasing concentrations (0.2–8 mM) of UDP

to UDP. The H12A mutant slightly affected the binding to UDP, indicating that its binding efficiency was approximately 1.6-fold lower than that of WT-MtCuvA (Fig. 4B), whereas S196A, T199A, N226A, and H298 mutants significantly reduced the binding efficiencies to UDP. The K_D values of S196A and T199A mutants were approximately 7- and threefold higher than that for WT-MtCuvA, respectively, and their binding efficiencies were approximately 7.5- and 4.2-fold lower than that of WT-MtCuvA, respectively (Fig. 4C and D). In particular, N226A and H298A mutants strongly affected the binding to UDP. These N226A and H298A mutants showed too low K_D and ΔT_m max values to estimate their binding efficiencies (Fig. 4E and F). Consequently, these results revealed that five residues, H12, S196, T199, N226, and H298, may be involved in the binding of UDP moiety at the putative ligand binding pocket of MtCuvA.

In conclusion, further studies remain to understand their interactions at molecular levels by determining a binary complex structure of MtCuvA with UDP-GlcNAc, but we identified key residues involved in the binding of UDP-GlcNAc to the putative ligand binding pocket of MtCuvA. Particularly, our results provide detailed information regarding the ligand binding properties of UDP-GlcNAc to MtCuvA including the binding orientation of UDP moiety in the putative ligand binding pocket of MtCuvA. A recent study in *B. subtilis* on cell wall homeostasis reported that GlmR, an orthologous protein of MtCuvA, might have a booster effect in a UDP-GlcNAc-dependent manner either on the activity of glucosamine-6-phosphate synthase (GlmS) required for UDP-GlcNAc synthesis or on that of YvcJ (corresponding to Rv1421 protein of *M. tuberculosis*) [14]. Besides, they have suggested that the characterization of the YvcJ role may provide clues with regard to functional triad proteins, YvcJ, GlmR, and GlmS, and the UDP-GlcNAc-dependent regulatory device for PG synthesis adapted to nutrient availability. Thus, nowadays, structural and biochemical studies of *M. tuberculosis* Rv1421 protein are in progress to elucidate its interaction with MtCuvA related to UDP-GlcNAc-dependent regulation.

Acknowledgements
Not applicable.

Author contributions
YCJ, JP and YJC carried out experiments. YCJ, JP and KSL designed experiments and analyzed data. YCJ and KSL wrote the manuscript. All authors read and approved the final manuscript.

Funding
This study was supported by Basic Science Research Program through the National Research Foundation of Korea (NRF) funded by the Ministry of Education (No. 2018R1D1A1B07047424) and was supported by the National Research Foundation of Korea (NRF) grant funded by the Korea government (MSIT) (No. 2021R1F1A1047349).

Availability of data and materials
Data sharing is not applicable to this article as no datasets were generated or analyzed during the current study.

Declarations

Ethics approval and consent to participate
Not applicable.

Consent for publication
Not applicable.

Competing interests
The authors declare that they have no competing interests.

Received: 13 October 2023 Accepted: 15 November 2023
Published online: 25 November 2023

References

1. Rohde K, Yates RM, Purdy GE, Russell DG (2007) *Mycobacterium tuberculosis* and the environment within the phagosome. Immunol Rev 219:37–54
2. Goossens SN, Sampson SL, Van Rie A (2020) Mechanisms of drug-induced tolerance in *Mycobacterium tuberculosis*. Clin Microbiol Rev 34(1):e00141
3. Banuls AL, Sanou A, Van Anh NT, Godreuil S (2015) *Mycobacterium tuberculosis*: ecology and evolution of a human bacterium. J Med Microbiol 64(11):1261–1269
4. Gomez JE, McKinney JD (2004) *M. tuberculosis* persistence, latency, and drug tolerance. Tuberculosis 84(1–2):29–44
5. Behr MA, Edelstein PH, Ramakrishnan L (2019) Is *Mycobacterium tuberculosis* infection life long? BMJ 367:l5770
6. Dulberger CL, Rubin EJ, Boutte CC (2020) The mycobacterial cell envelope - a moving target. Nat Rev Microbiol 18(1):47–59
7. Nogrado K, Unno T, Hur HG, Lee JH (2021) Tetracycline-resistant bacteria and ribosomal protection protein genes in soils from selected agricultural fields and livestock farms. Appl Biol Chem 64(1):42
8. Pandey AK, Sassetti CM (2008) Mycobacterial persistence requires the utilization of host cholesterol. Proc Natl Acad Sci USA 105(11):4376–4380
9. Ehrt S, Schnappinger D, Rhee KY (2018) Metabolic principles of persistence and pathogenicity in *Mycobacterium tuberculosis*. Nat Rev Microbiol 16(8):496–507
10. Brzostek A, Pawelczyk J, Rumijowska-Galewicz A, Dziadek B, Dziadek J (2009) *Mycobacterium tuberculosis* is able to accumulate and utilize cholesterol. J Bacteriol 191(21):6584–6591
11. Mir M, Prisic S, Kang CM, Lun S, Guo H, Murry JP, Rubin EJ, Husson RN (2014) Mycobacterial gene *cuvA* is required for optimal nutrient utilization and virulence. Infect Immun 82(10):4104–4117
12. Jeong YC, Lee KS (2020) A proposed carbon-utilization and virulence protein A, CuvA (Rv1422), from *Mycobacterium tuberculosis* H37Rv: crystallization, X-ray diffraction analysis and ligand binding. Acta Crystallogr F Struct Biol Commun 76(Pt 7):314–319
13. Foulquier E, Galinier A (2017) YvcK, a protein required for cell wall integrity and optimal carbon source utilization, binds uridine diphosphate-sugars. Sci Rep 7(1):4139
14. Foulquier E, Pompeo F, Byrne D, Fierobe HP, Galinier A (2020) Uridine diphosphate *N*-acetylglucosamine orchestrates the interaction of GlmR with either YvcJ or GlmS in *Bacillus subtilis*. Sci Rep 10(1):15938
15. Foulquier E, Pompeo F, Bernadac A, Espinosa L, Galinier A (2011) The YvcK protein is required for morphogenesis via localization of PBP1 under gluconeogenic growth conditions in *Bacillus subtilis*. Mol Microbiol 80(2):309–318
16. Kang CM, Abbott DW, Park ST, Dascher CC, Cantley LC, Husson RN (2005) The *Mycobacterium tuberculosis* serine/threonine kinases PknA and PknB: substrate identification and regulation of cell shape. Genes Dev 19(14):1692–1704

17. Robert X, Gouet P (2014) Deciphering key features in protein structures with the new ENDscript server. Nucleic Acids Res 42(Web Server issue):W320–W324
18. Cramer P (2021) AlphaFold2 and the future of structural biology. Nat Struct Mol Biol 28(9):704–705
19. Arnold K, Bordoli L, Kopp J, Schwede T (2006) The SWISS-MODEL workspace: a web-based environment for protein structure homology modelling. Bioinformatics 22(2):195–201
20. Murail S, de Vries SJ, Rey J, Moroy G, Tuffery P (2021) SeamDock: an interactive and collaborative online docking resource to assist small compound molecular docking. Front Mol Biosci 8:716466
21. Trott O, Olson AJ (2010) AutoDock Vina: improving the speed and accuracy of docking with a new scoring function, efficient optimization, and multithreading. J Comput Chem 31(2):455–461
22. Schrodinger, LLC (2010) The PyMOL Molecular Graphics System, Version 1.3r1.
23. Braman J, Papworth C, Greener A (1996) Site-directed mutagenesis using double-stranded plasmid DNA templates. Methods Mol Biol 57:31–44
24. Patel V, Wu Q, Chandrangsu P, Helmann JD (2018) A metabolic checkpoint protein GlmR is important for diverting carbon into peptidoglycan biosynthesis in *Bacillus subtilis*. PLoS Genet 14(9):e1007689

Publisher's Note